Optimizing angular diSPIM measurements

February 21, 2019

1 Introduction

Our goal in these notes is to find optimal angular sampling schemes for the diSPIM with light-sheet tilting. We review the continuous angular forward model, find the sampling schemes available to us, choose an objective function to optimize, then search through the sampling schemes.

2 Continuous forward model

We briefly review the continuous angular forward model—see the previous notes for a more detailed discussion. We can write the continuous-to-continuous forward model in the form

$$\mathbf{g}_c = \mathcal{H}_{cc}\mathbf{f}_c, \tag{1}$$

where $\mathbf{f}_c \in \mathbb{L}_2(\mathbb{S}^2)$ is the angular dipole density, $\mathbf{g}_c \in \mathbb{L}_2(\mathbb{S}^2 \times \mathbb{S}^1)$ is the continuous irradiance data taken by varying the detection optical axis (the $\mathbb{S}^2$ dimension) and the illumination polarizer (the $\mathbb{S}^1$ dimension), and $\mathcal{H}_{cc}$ is a linear continuous-to-continuous Hilbert-space operator between these spaces.

If we choose a delta-function basis for both object and data space then we can rewrite Eq. (1) as

$$g(\hat{\mathbf{s}}_d, \hat{\mathbf{p}}) = \int_{\mathbb{S}^2} d\hat{\mathbf{s}}_o \, h(\hat{\mathbf{s}}_d, \hat{\mathbf{p}}; \hat{\mathbf{s}}_o) f(\hat{\mathbf{s}}_o), \tag{2}$$

where $\hat{\mathbf{s}}_o \in \mathbb{S}^2$ is the object angular coordinate, $\hat{\mathbf{s}}_d \in \mathbb{S}^2$ is the detection optical axis coordinate, $\hat{\mathbf{p}} \in \mathbb{S}^1$ is the polarizer coordinate, and $h(\hat{\mathbf{s}}_d, \hat{\mathbf{p}}; \hat{\mathbf{s}}_o)$ is the kernel of the integral transform. We can separate the kernel into an excitation and detection part since these processes are incoherent

$$h(\hat{\mathbf{s}}_d, \hat{\mathbf{p}}; \hat{\mathbf{s}}_o) = h^{\text{exc}}(\hat{\mathbf{p}}; \hat{\mathbf{s}}_o) h^{\text{det}}(\hat{\mathbf{s}}_d; \hat{\mathbf{s}}_o). \tag{3}$$

The excitation kernel is straightforward—the squared dot product of the polarizer orientation $\hat{\mathbf{p}}$ with the object angular coordinate $\hat{\mathbf{s}}_o$

$$h^{\text{exc}}(\hat{\mathbf{p}} \cdot \hat{\mathbf{s}}_o) \propto (\hat{\mathbf{p}} \cdot \hat{\mathbf{s}}_o)^2. \tag{4}$$

The detection kernel requires more care since we are collecting light over the NA of the objective. In the previous notes we started with the power along a single ray then integrated over the aperture to find that the detection kernel is

$$h^{\text{det}}(\hat{\mathbf{s}}_d \cdot \hat{\mathbf{s}}_o) \propto 2(1 - \sqrt{\cos\alpha}) P_0(\hat{\mathbf{s}}_d \cdot \hat{\mathbf{s}}_o) + \frac{1}{5}\left[\frac{2}{5} + \frac{1}{10}\sqrt{\cos\alpha}(-7 + 3\cos\alpha)\right] P_2(\hat{\mathbf{s}}_d \cdot \hat{\mathbf{s}}_o), \tag{5}$$

where $\text{NA} = n_o \sin\alpha$, and $P_\ell(x)$ are the Legendre polynomials.

We can rewrite the mapping in Eq. (1) in an object-space spherical harmonic basis as

$$g(\hat{\mathbf{s}}_d, \hat{\mathbf{p}}) = \sum_{\ell m} H_\ell^m(\hat{\mathbf{s}}_d, \hat{\mathbf{p}}) F_\ell^m, \tag{6}$$

where F_ℓ^m is the angular dipole spectrum given by

$$F_\ell^m = \int_{\mathbb{S}^2} d\hat{\mathbf{s}}_o \, f(\hat{\mathbf{s}}_o) Y_\ell^{m*}(\hat{\mathbf{s}}_o), \tag{7}$$

and $H_\ell^m(\hat{\mathbf{s}}_d, \hat{\mathbf{p}})$ is the kernel in this basis given by

$$H_\ell^m(\hat{\mathbf{s}}_d, \hat{\mathbf{p}}) = \sum_{\ell' m'} \sum_{\ell'' m''} (-1)^m G_{\ell,\ell',\ell''}^{-m,m',m''} H_{\ell'}^{m',\text{exc}}(\hat{\mathbf{p}}) H_{\ell''}^{m'',\text{det}}(\hat{\mathbf{s}}_d), \tag{8}$$

$$H_{\ell'}^{m',\text{exc}}(\hat{\mathbf{p}}) \propto Y_{\ell'}^{m'*}(\hat{\mathbf{p}}) \left[\delta_{0\ell'} + \frac{2}{5} \delta_{2,\ell'} \right], \tag{9}$$

$$H_{\ell''}^{m'',\text{det}}(\hat{\mathbf{s}}_d) \propto \frac{Y_{\ell''}^{m''*}(\hat{\mathbf{s}}_d)}{1 - \cos\alpha} \left[(1 - \sqrt{\cos\alpha}) \delta_{0,\ell''} + \left(\frac{2}{5} + \frac{1}{10} \sqrt{\cos\alpha} (-7 + 3\cos\alpha) \right) \delta_{2,\ell''} \right]. \tag{10}$$

with the Gaunt coefficients given by

$$G_{\ell,\ell',\ell''}^{m,m',m''} = \int_{\mathbb{S}^2} d\hat{\mathbf{s}}_o \, Y_\ell^m(\hat{\mathbf{s}}_o) Y_{\ell'}^{m'}(\hat{\mathbf{s}}_o) Y_{\ell''}^{m''}(\hat{\mathbf{s}}_o). \tag{11}$$

It's useful to compare Eq. (2) to Eq. (6)—in a delta function basis we need to compute an angular integral, while in the object-space spherical harmonics basis the kernel has a finite number of terms so we can compute it exactly.

It's also useful to compare Eq. (3) to Eq. (8)—in a delta function basis the kernel is the product of the excitation and detection kernels, while in the object-space spherical harmonic basis the kernel is a generalized convolution of the excitation and detection kernels.

3 Sampling schemes

We can write the sampling operation as a continuous-to-discrete Hilbert space operator $\mathcal{D}_w$

$$\mathbf{g}_d = \mathcal{D}_w \mathbf{g}_c = \mathcal{D}_w \mathcal{H}_{cc} \mathbf{f}_c. \tag{12}$$

We can write the sampling operation in a delta function basis as

$$g_m = \int_{\mathbb{S}^2} d\hat{\mathbf{s}}_d \int_{\mathbb{S}^1} d\hat{\mathbf{p}} \, w_m(\hat{\mathbf{s}}_d, \hat{\mathbf{p}}) g(\hat{\mathbf{s}}_d, \hat{\mathbf{p}}). \tag{13}$$

where g_m is the mth discrete measurement and $w_m(\hat{\mathbf{s}}_d, \hat{\mathbf{p}})$ is the mth sampling aperture. For now we will restrict ourselves to delta-function sampling apertures

$$w_m(\hat{\mathbf{s}}_d, \hat{\mathbf{p}}) = \delta(\hat{\mathbf{s}}_{d,m} - \hat{\mathbf{s}}_d) \delta(\hat{\mathbf{p}}_m - \hat{\mathbf{p}}), \tag{14}$$

where $\hat{\mathbf{s}}_{d,m}$ and $\hat{\mathbf{p}}_m$ are the mth sampling points. This restriction means that we will leave the polarizer setting and tilt angle fixed during each volume acquisition. We could consider scanning the polarizer setting and tilt angle in the future for faster acquisitions, but I think these sampling schemes will always decrease "angular SNR".

So far we've formulated everything quite generally and haven't made any reference to the diSPIM geometry. Now we find the constraints that the diSPIM geometry places on the values of $\hat{\mathbf{s}}_{d,m}$ and $\hat{\mathbf{p}}_m$. If we define the $\hat{\mathbf{x}}$ and $\hat{\mathbf{z}}$ axes as the optical axes of the two objective then we have the following sampling constraint

$$\hat{\mathbf{s}}_{d,m} \in \{\hat{\mathbf{x}}, \hat{\mathbf{z}}\}. \tag{15}$$

In words, this constraint says that we can only detect along one of two discrete and orthogonal axes.

Next, we constrain the polarizer sampling points $\hat{\mathbf{p}}_m$. We introduce a variable $\hat{\mathbf{s}}_{e,m}$ to denote the excitation optical axis for the mth measurement. This variable does not affect the forward model (we've formulated in

terms of $\hat{\mathbf{p}}$ only on the excitation side), but it will allow us to conveniently constrain $\hat{\mathbf{p}}$. First, we constrain the excitation optical axis to be perpendicular to the detection optical axis

$$\hat{\mathbf{s}}_{e,m} \cdot \hat{\mathbf{s}}_{d,m} = 0. \tag{16}$$

This is a fairly loose constraint, but it ensures that the light sheet is in focus across the field of view.

Next, we constrain the excitation optical axis to within the available tilt angles of the instrument. If we use $\mathcal{R}$ to denote an "axis swapping operator" ($\mathcal{R}(\hat{\mathbf{z}}) = \hat{\mathbf{x}}$ and $\mathcal{R}(\hat{\mathbf{x}}) = \hat{\mathbf{z}}$), then the tilting constraint can be written as

$$\hat{\mathbf{s}}_{e,m} \cdot \mathcal{R}(\hat{\mathbf{s}}_{d,m}) \leq \Delta, \tag{17}$$

where Δ is the maximum tilt angle. For the current instrument $\Delta = 15^\circ = \pi/12$.

Finally, we constrain the excitation polarization $\hat{\mathbf{p}}_m$ to be perpendicular to the excitation optical axis

$$\hat{\mathbf{s}}_{e,m} \cdot \hat{\mathbf{p}}_m = 0. \tag{18}$$

For convenience we will denote individual sampling points with $\mathfrak{s}_m = (\hat{\mathbf{p}}_m, \hat{\mathbf{s}}_{d,m})$, and we will denote the set of all sampling points $\mathfrak{s}_m$ that satisfy Eqs. (15)–(18) by $\mathcal{S}$. With this notation we can denote a complete sampling scheme with M samples by $\mathfrak{s} \in \mathcal{S}^M$ (M copies of the set $\mathcal{S}^M$).

4 Objective functions

Our goal is to choose an M-sample sampling scheme $\mathfrak{s} \in \mathcal{S}^M$ that is optimal in some sense. We propose that we minimize the $\mathbb{L}_2$ condition number of the continuous-to-discrete imaging operator—the ratio of the largest and smallest singular values of the matrix. We can interpret the condition number as the "invertibility" of the matrix.

Optimizing the condition number will generate designs that are easily inverted, but the designs may estimate a small number of uninteresting parameters. For this reason we impose a rank constraint on the matrix. We require that

$$\operatorname{rank}(\mathcal{D}_{\mathfrak{s}}\mathcal{H}_{cc}\mathcal{P}_{\ell_c=2}) \geq 6, \tag{19}$$

where $\mathcal{P}_{\ell_c=2}$ is a projection operator onto the $\ell = 0$ and $\ell = 2$ subspace. For convenience we will denote the set of sampling schemes that satisfy the constraint in Eq. (19) by $\mathcal{Z} = \{\mathfrak{s} \,|\, \operatorname{rank}(\mathcal{D}_{\mathfrak{s}}\mathcal{H}_{cc}\mathcal{P}_{\ell_c=2}) \geq 6\}$. An optimal M-sample sampling scheme will be the solution of the optimization problem

$$\mathfrak{s}^* = \underset{\mathfrak{s} \in \mathcal{S}^M \cap \mathcal{Z}}{\operatorname{argmin}} \, \kappa(\mathcal{D}_{\mathfrak{s}}\mathcal{H}_{cc}), \tag{20}$$

where $\kappa(A)$ denotes the $\mathbb{L}_2$ condition number of A.

Earlier we mainly used the Schatten 2-norm of the continuous-discrete imaging operator—the root sum of squares of the singular values—as the objective function. This objective function resulted in useful designs, but the last singular value was usually small which led us to optimizing the condition number. We can interpret the Schatten 2-norm designs as the "learn as much as we can about all parameters" designs and the condition number designs as the "no parameter left behind" designs.

5 Practical implementation details

The optimization problem above lacks many of the details required for an implementation. In this section I'll go through some of the practical work of converting the abstract form into a finite-dimensional optimization problem.

First, we need to choose a basis and find matrix representations for the operators $\mathcal{D}_{\mathfrak{s}}$ and $\mathcal{H}_{cc}$. At first glance this seems difficult—$\mathcal{D}_{\mathfrak{s}}$ is a CD operator and $\mathcal{H}_{cc}$ is a CC operator so they do not have finite-dimensional matrix representations individually. Luckily, the combination $\mathcal{D}_{\mathfrak{s}}\mathcal{H}_{cc}$ is a band-limited compact operator, so it has a finite-dimensional representation as a $15 \times M$ matrix that we will call H. The entries of this matrix are given by

$$\mathsf{H}_{jm} = H_j(\hat{\mathbf{s}}_{d,m}, \hat{\mathbf{p}}_m), \tag{21}$$

where j is a single index over the spherical harmonics, and Eq. 8 shows us how to calculate the entries in terms of the excitation and detection kernels.

Next, we need a matrix representation of $\mathcal{P}_{\ell_c=2}$. This is simple in a spherical harmonics basis—we create a 15×15 matrix called P, fill the first six diagonal elements with ones, and place zeroes elsewhere

$$\mathsf{P}_{ij} = \delta_{ij}, \qquad i,j = 0,1,2,3,4,5. \tag{22}$$

Finally, we need an efficient set of scalar parameters to search through the set of sampling schemes $\mathcal{S}^M$. We will parameterize each sample with a discrete view index $v \in \{0,1\}$ to indicate the detection axis, a tilt angle defined from the nominal excitation axis $\delta \in [-\Delta, \Delta]$, and a polarizer angle defined from the detection axis $\phi \in [0, 2\pi)$.

This parameter space is challenging to search because it is continuous in some parameters and discrete in others. It's not clear if it's possible to take derivatives with respect to the continuous parameters, so as a first pass we will discretize the continuous parameters and use a search heuristic. Discretization has the advantage of providing solutions that will be easier to implement experimentally since we can constrain our solutions to sampling schemes that are easy to align, but of course we can't guarantee that our sampling scheme solutions will be globally optimal.

We will discretize the tilt angle into 3 angles $\delta \in \{-\Delta, 0, \Delta\}$, and we will discretize the polarizer angle into P angles $\phi \in \{0, \pi/P, \ldots, (P-1)\pi/P\}$. This means that a brute-force approach will need to search the number of ways to choose M elements from 2 views $\times$ 3 tilts $\times$ P polarizer options $= \binom{6P}{M}$.

My current implementation requires about 2 milliseconds per objective function evaluation, so a brute force search is feasible for $P = 6$ and $M = 6$ since $\binom{36}{6} \approx 2 \times 10^6$ evaluations will take about 2 hours.

6 Results

Figure 1–3 include several subfigures that we can use to compare the designs.

In the **top left** subfigure we show a schematic of the angular design. Each arrow indicates a single polarized excitation direction and tilt angle. In the current diSPIM design we do not use any excitation arm tilting, so all 6 arrows are centered on the optic axes (indicated by large black dots). The colors of the arrows match the small colored squares in the **top center** subfigure which indicate the point response functions for each measurement. The radius of each point response function indicates the size of the signal measured from a fluorophore oriented along that direction.

In the **top right** subfigure we show an set of single direction reconstructions with the given design. We start by creating a uniformly oriented phantom for each of the 250 directions in the positive octant of the sphere indicated by green dots. Next, we simulate the imaging process, simulate Poisson noise with SNR = 20, reconstruct the phantom, then find maximum of the reconstructed ODF. We mark each reconstructed maximum with a red dot and connect each phantom/reconstruction pair with a black line.

In the **center** subfigure we show the singular value spectrum of the imaging system with the singular vectors plotted on the x axis. The singular vectors are orthogonal functions, so they necessarily have positive (red)

and negative (blue) components. In the top-right of the figure we show the Schatten 2-norm of the design, the condition number, and the rank.

In the **bottom** subfigure we show the singular value spectrum of the imaging system after projecting onto the $\ell = 0, 2$ subspace with the associated Schatten 2-norm, condition number, and rank.

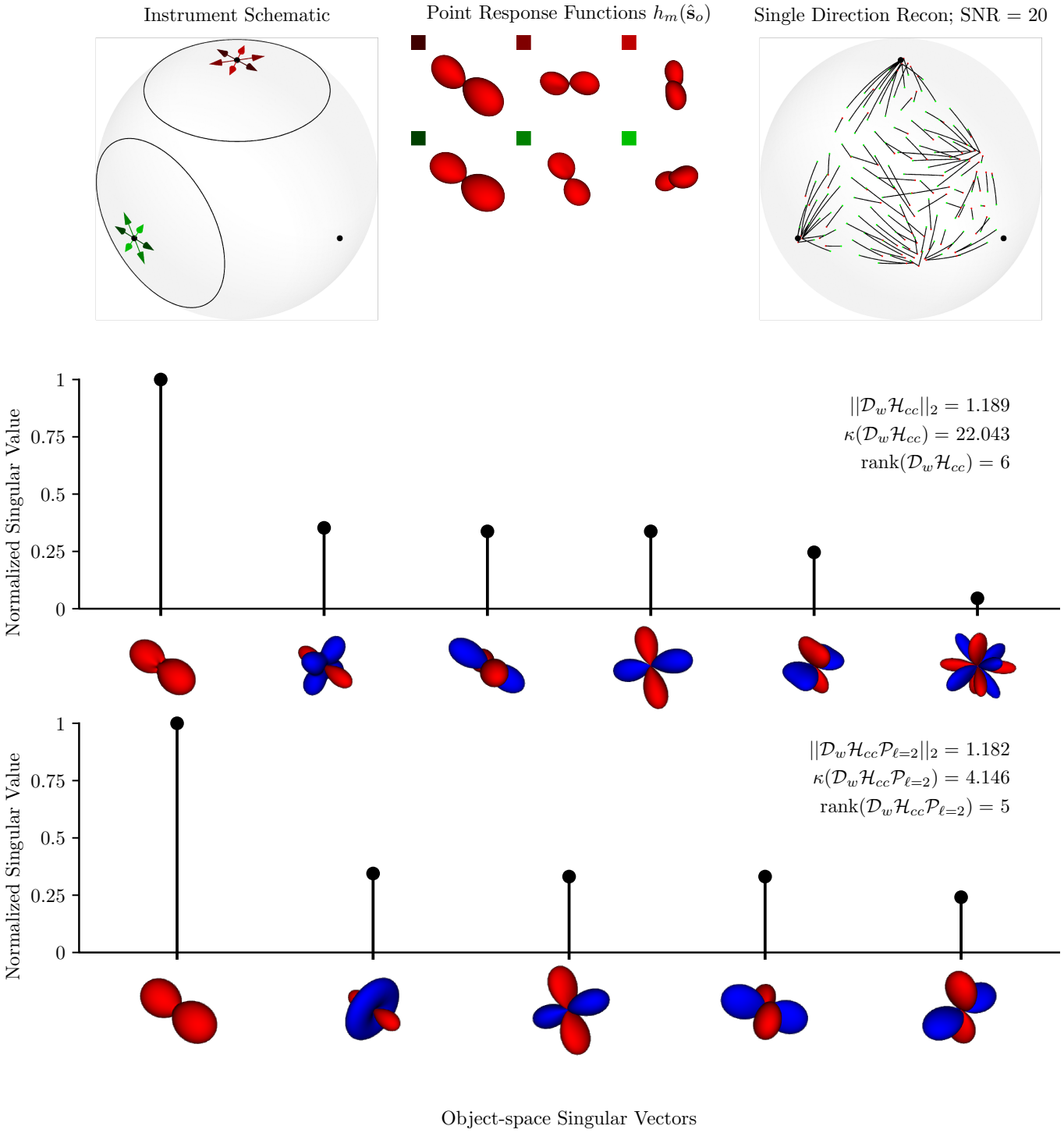

Figure 1: 3-polarization diSPIM design. See the top of Section 6 for the general caption. The current design does not use any light sheet tilting, so the arrows in the schematic are centered on the black dots. Although the 3-polarization diSPIM design measures a 6-dimensional space (its rank is 6), the last singular value is very small (1/22 of the maximum singular value) so it is effectively lost in the noise. The 3-polarization diSPIM design only measures a 5-dimensional subspace of the $\ell = 0, 2$ subspace, so the reconstructions suffer from significant blind spots. The single direction reconstructions show that many directions are reconstructed with errors larger than 30 degrees.

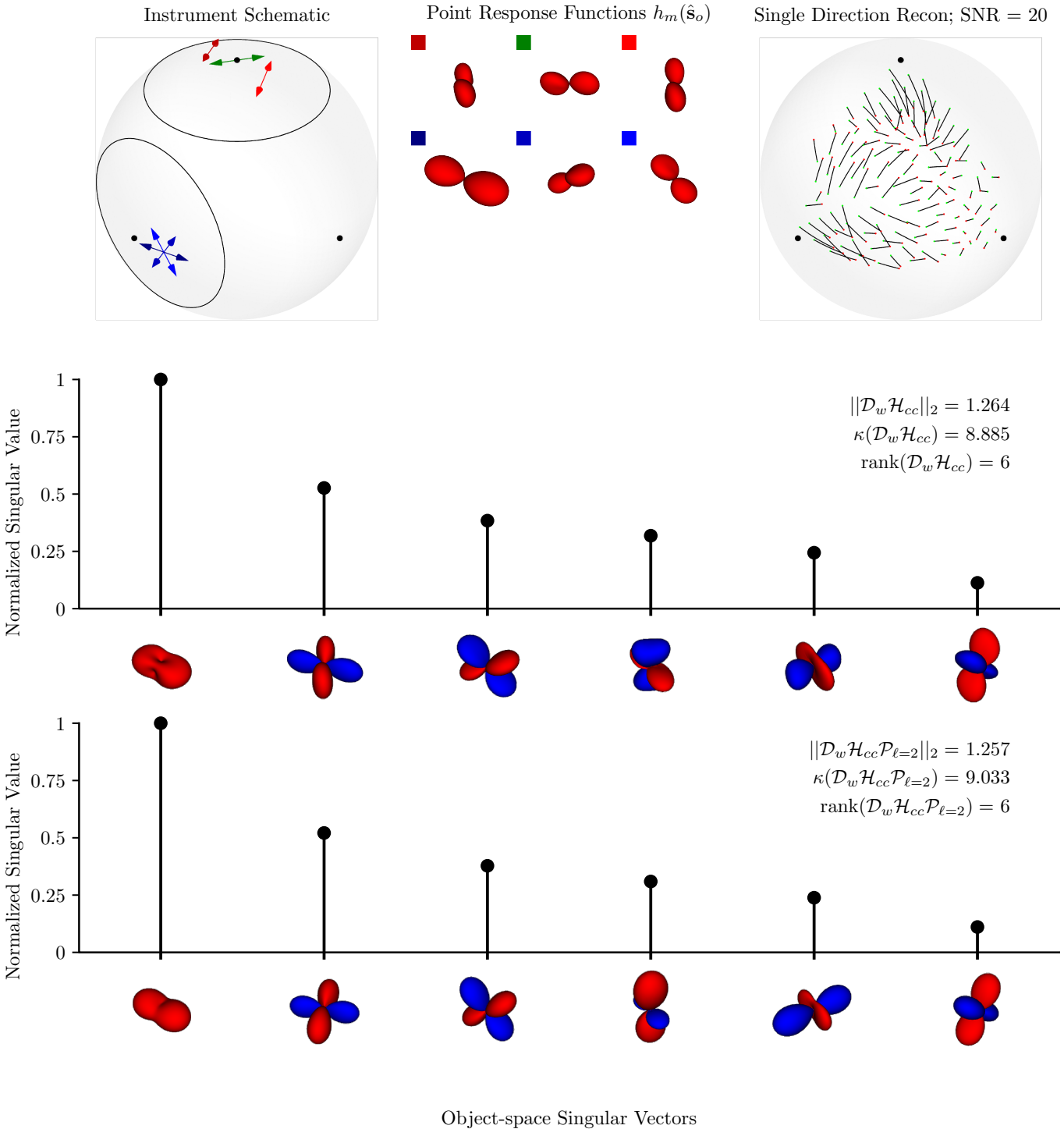

Figure 2: Optimal $M = 6$, $P = 3$ tilting diSPIM design. See the top of Section 6 for the general caption. This design is the optimal 6-measurement design when 3 equally spaced polarizer settings and light-sheet tilting are available. First, collect the blue samples by tilting the light sheet and cycling through the three polarizer settings. Next, collect the red samples from the other view by choosing the polarizer setting that points towards blue excitation axis and tilting the excitation sheet both directions. Finally, collect the green sample by changing the polarizer setting and exciting along the optic axis. This design shows several advantages over our current design: the smallest singular value is 1/9 the size of the largest singular value, so we have a much better chance of recovering it from the noise; we measure components from all 6 dimensions of the $\ell = 0, 2$ subspace; and the single direction reconstruction shows that we can reconstruct with errors less than 15 degrees.

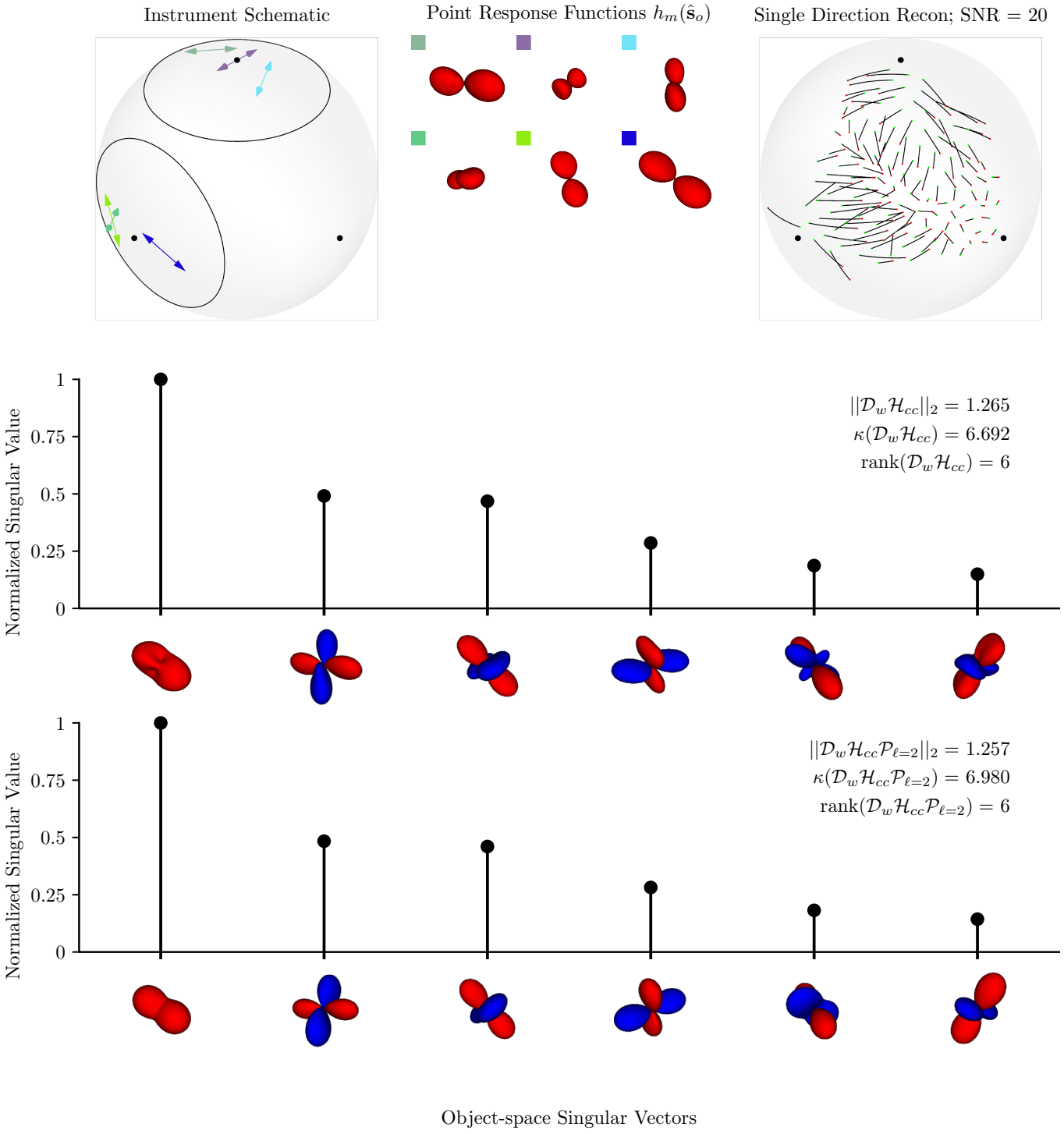

Figure 3: Optimal $P = 6$ tilting diSPIM design. See the top of Section 6 for the general caption. This design is the optimal 6-measurement design when 6 equally spaced polarizer settings and light-sheet tilting are available. Compared to the optimal $P = 3$ design in Figure 2, the optimal $P = 6$ design has a smallest singular value that is 1/7 the size of the largest singular value, so it is even less susceptible to corruption by noise. Interestingly, the singular direction reconstruction looks worse for the $P = 6$ design than the $P = 3$ design. This isn't too troubling since we have optimized on the condition number, not the single direction reconstruction. Although this design has a slightly better condition number, it requires finer polarization alignment than the $P = 3$ design, it requires tilting on both arms, and it does not provide a very large improvement. With these comments and the "Min constraint" in mind, I'm happy to recommend the $P = 3$ design.